JAERI-M
90-081

DENSITY LIMIT IN JT-60

May 1990

Yutaka KAMADA, Nobuyuki HOSOGANE
Toshio HIRAYAMA and Toshihide TSUNEMATSU

日 本 原 子 力 研 究 所
Japan Atomic Energy Research Institute

JAERI Mレポートは，日本原子力研究所が不定期に公刊している研究報告書です。
入手の問合わせは，日本原子力研究所技術情報部情報資料課（〒319 11 茨城県那珂郡東海村）あて，お申しこしください。なお，このほかに財団法人原子力弘済会資料センター（〒319 11 茨城県那珂郡東海村日本原子力研究所内）で複写による実費領布をおこなっております。

JAERI M reports are issued irregularly.
Inquiries about availability of the reports should be addressed to Information Division Department of Technical Information, Japan Atomic Energy Research Institute, Tokaimura, Naka gun, Ibaraki ken 319 11, Japan.

編集兼発行　日本原子力研究所
印　　刷　ニッセイエブロ株式会社

JAERI-M 90-081

Density Limit in JT-60

Yutaka KAMADA, Nobuyuki HOSOGANE, Toshio HIRAYAMA
and Toshihide TSUNEMATSU

Department of Large Tokamak Research
Naka Fusion Research Establishment
Japan Atomic Energy Research Institute
Naka-machi, Naka-gun, Ibaraki-ken

(Received April 12, 1990)

This report studies mainly the density limit for a series of gas- and pellet-fuelled limiter discharges in JT-60. With the pellet injection into high-current/low-q ($q(a)=2.3\sim2.5$) discharges, the Murakami factor reaches up to $10\sim13\times10^{19}m^{-2}T^{-1}$. The values are about factors of $1.5\sim2.0$ higher than those for usual gas-fuelled discharges. The pellet injected discharges have high central density, whereas the electron density in the outer region ($a/2<r$) is limited below the same level with that for gas fuelled plasmas. The density limit can be explained with the power balance in the outer region of the plasma, for which the plasma purity (Zeff), heating power and the electron temperature are the key parameters. The disruptive limit of the density can be explained by P_{abs} and $n_e^2(r=50cm)\times Z_{eff}(r=50cm)$.

Keywords: JT-60, Density Limit, Pellet Injection, Gas Puff,
Edge Electron Density, Z_{eff}

JT－60における密度限界

日本原子力研究所那珂研究所臨界プラズマ研究部
鎌田　裕・細金　延幸・平山　俊雄
常松　俊秀

（1990年4月12日受理）

JT－60のリミター配位における密度限界について，一連のガスパフ及びペレット入射実験結果を用いて議論する。ペレット入射によって得られた村上係数は，ガスパフ時の1.5～2倍である。また，ペレット入射時における最大の村上係数は10～13×$10^{19}$$m^{-2}$$T^{-1}$であり，これは高プラズマ電流／低q（q(a)≒2.3～2.5）放電時に得られた。このようなペレット入射によって形成される電子密度分布はプラズマ中心で高い値を持つが，一方周辺部（a/2<r）では，ガスパフ時と同程度の値となっている。これらのガスパフ及びペレット入射実験結果により，密度上限はプラズマ周辺部でのパワーバランスによって理解出来ることが分かった。この時，Zeff，加熱パワー，周辺電子温度が重要なパラメーターである。

東海研究所：〒319－11　茨城県那珂郡東海村白方字白根2－4

Contents

目　　次

1.Introduction

The density range and the profile play the most important roles to optimize the reasonable reactor concept. They affect the plasma performance in all aspects, viz. confinement characteristics, plasma purity, fusion output, heat deposition, current drive efficiencies, wall (divertor plate) load, disruption properties, ash exhaust, pumping rate etc. Therefore, intrinsically, there are many ' density limits' for different physical and engineering aspects. One of the key limits of the density, this report studies the density limit for disruption. To emphasize the role of the power balance in the outer region (a/2<r) of the plasma, we analyzed a series of gas- and pellet-fuelled limiter discharges in JT-60.

JT-60 uses a pellet injector to study the density-related characteristics of the plasma. With the pellet injection, energy confinement time was enhanced up to 40% relative to usual gas fuelled discharges and the strongly peaked electron density profile with the peaking factor (central value / volume averaged value) $n_e(0)/\langle n_e\rangle$ <4.5 was obtained for medium current of Ip=2.1MA (q(a)=3.3) [1,2]. For the highest plasma current of 3.1MA (q(a)=2.3), $n_e(0)/\langle n_e\rangle$ <3 and $n_e(0)<2.7\times10^{20}m^{-3}$ was sustained within 0.5-1 sec after a series of pellet injection. For a series of 3.1MA discharges, central plasma pressure reaches 2 atm. and achieved values of $n_e(0)T_i(0)\tau_E$ ($<1.2\times10^{20}m^{-3}$sec keV) is two times larger than those obtained with gas-puffing. For well center-fuelled discharges, the sawtooth activity is suppressed. Improved energy confinement for the pellet fuelled plasma is mainly due to the peaked density and pressure profiles inside the q=1 rational surface, where the confinement characteristics appear to be better than those in the outer (q>1) region [1,2]. The pressure gradient of discharges with a center peaked density profile reaches locally the marginal value for the infinite-n ballooning mode inside r_s. The total pressure inside r_s (or the poloidal beta within r_s, β_{p1}) has not reached the ideal ballooning limit optimized for all position inside r_s. The analysis with ERATO-code shows that the attained maximum β_{p1} is consistent with the internal n=1 kink mode beta limit [3].

This report is arranged as follows: In Section 2, the experimental setup of the JT-60 device, diagnostics related to this report, discharge conditions are briefly described. Section 3 deals with the density limit for disruption. In Section 4, MARFE limit in JT-60 is discussed. In Section 5, the fuelling efficiencies for gas- and pellet-fuelling are compared. Section 6 presents the conclusion.

2. Experimental Set-up and Discharge Conditions

Recent JT-60 experiments use limiter and lower x-point configurations (shown in Fig.1)[4]. The typical limiter configuration (Fig.1(b)) has an almost circular cross section and the major and the minor radii (R and a) are 3.05m and 0.9m. For the lower x-point divertor configuration, R~3m, averaged minor radius~0.7m and the plasma elongation~1.3~1.4. The main working gas is hydrogen. The operational region of the discharges are: Ip<3.1MA (limiter), Ip<2.0MA (divertor) , Bt<4.8T and NBI power <25MW. The first wall and the divertor plates are covered with carbon tiles.

A four-barrel pneumatic pellet injector installed on JT-60 produces cylinder-shaped hydrogen pellets with velocities approaching 2.3km/sec, with which two small and two large pellets can be fired independently . Sizes of the pellets are 3.0mmϕ(in diameter) ×3.0mm^{l} (in length) and 4.0mmϕ×4.0mm^{l}. The small and large pellets contain 0.96×10^{21} and 2.3×10^{21} atoms, respectively. The averaged fuelling efficiency of each pellet is about 70~80% of the particle inventory determined by the ideal pellet dimensions and the remaining particles are lost in the formation and acceleration phases. The pellets are injected with an angle of 47 degree from the midplane. The injection trajectory is off-axis and the nearest distance from the geometric center of the torus is 12cm. The ablation profiles of injected pellets are monitored by a 7-channel H_α detector array using fiber optics with time response of 1μsec. The line of sight of each detector, the geometry of the pellet injector, chords of a Thomson scattering system and a FIR interferometer are shown in Fig.1(a). With the FIR interferometer (the chord is 50cm off-axis from the geometric center of the vacuum vessel), the line averaged electron density in the outer region can be measured. Figure 1(b) shows the limiter configuration and lines of sight of a lower half set of soft X-ray (SX) detectors (PIN diode array). Figure 1(c) gives the lines of sights for bolometer arrays for the measurement of the radiated power.

Figure 2 shows electron density profiles for pellet fuelled limiter discharges. With the pellet injection, the strongly peaked electron density profile with the peaking factor (central value / volume averaged value) $n_e(0)/\langle n_e\rangle$ <4.5 was obtained for medium current of Ip=2.1MA (q(a)=3.3) (Fig.2(a)). Figure 2(b) gives an example for $n_e(r)$ for a 3.1MA (q(a)=2.3) limiter discharge, where $n_e(0)/\langle n_e\rangle$ <3 and $n_e(0)<2.7\times10^{20}m^{-3}$ was sustained within 0.5-1 sec after a series of pellet injection. In Fig.2(b), $n_e(r)$ for a gas fuelled discharge is shown. In the outer region, n_e for the pellet-fuelled discharge is not highly increased compared to that in the gas-fuelled case. For well center-fuelled discharges in JT-60, the sawtooth activity is suppressed and the particle confinement in the q<1 region is better than that in the outer region, therefore, the produced density profile has a highly peaked portion inside the q=1 surface.

3. Density Limit

3.1 Operational Region for Gas Fuelled Plasmas on the Hugill Diagram

Figure 3 gives the operational region for gas fuelled plasmas on the Hugill diagram. Figure 3(a) indicates the operational region for limiter and divertor discharges without disrupted data. The upper boundary of n_e is written by $n_e=17\times10^{19}B_t/(Rq)$. In Fig.3(b), the disrupted data (closed symbols) are plotted on the stable data. The disrupted data diffuse in the whole operational region.

3.2 Operational Region for Pellet Fuelled Plasmas on the Hugill Diagram

The operational region for pellet fuelled limiter discharges are superimposed on that for the gas fuelled discharges in Fig.4. With the pellet injection into high-current / low-q (q(a)=2.3~2.5) discharges, the Murakami factor reaches up to $10\sim13\times10^{19}m^{-2}T^{-1}$. The values are about factors of 1.5~2.0 higher than those for usual gas-fuelled discharges.

In Figure 5(a), line averaged electron density for the 50cm-off-axis chord, $n_e(r=50cm)$, is used to indicate the operational region. Figure 5(b) compares the line averaged n_e for the central and the off-axis chords in the range of $2.3<q(a)<3.3$. For gas-fuelled discharges (closed circles), $n_e(r=0)$ is about $1.05\sim1.1\times n_e(r=50cm)$. For pellet fuelled discharges, $ne(r=0)\sim1.1\sim2\times n_e(r=50cm)$. Therefore, when the operational region is plotted using $n_e(r=50cm)$, the pellet data are gathered close to the gas-fuelled data as shown in Fig.5(a).

Figure 6 shows n_e profiles for 2.8MA limiter discharges measured just (0.02sec) after the pellet injection. E10243 was stable and E10237 disrupted at 0.1 sec after the pellet injection. The pellet penetration for E10237 was shallower than that for E10243. E10237 had higher NBI power and lower $n_e(r=0)$ compared to E10243, however E10237 disrupted and E10243 was stable. In both cases Z_{eff} was 1.85. The reason of the disruption for E10237 is considered that the discharge had higher density in the outer region.

These facts suggest that the operational region can be totally understood using n_e in the outer region of the plasma.

3.3 nRq/Bt vs. Pabs and Zeff

Figure 7 uses gas- and pellet- fuelled limiter discharges with Ip=2.8~3.1MA, Bt=4.5~4.8T and q(a)=2.3~2.4. In Figures 7(a) and (b), $n_e(r=50cm)Rq/Bt$ is plotted against absorbed power, P_{abs}, and Z_{eff} averaged along the 50cm-off-axis chord. Disrupted (in the Ip flat-top phase) and stable discharges are indicated with closed and open circles, respectively. With this data set, the density limit is discussed in the following sections. In Fig.7(a), the upper limit of the stable operation (broken line) traces with $\sim P_{abs}^{0.5}$. However, the disrupted data scatter in the lower density region.

3.4 Time Evolution of the Density Limit Disruption

As N.Hosogane reported [5], the density limit disruption in JT-60 evolves along the following scenario in the early phase of the disruption; i) edge-cooling occurs, ii) m=2 and/or m=3 modes glow, iii) edge-cooling evolves further and the MHD modes glow rapidly, iv) kinetic energy in r>r(q=1.5) region is released . Figure 8 shows a time evolution of the density limit disruption for a 2.1MA limiter discharge, in this case the pellets were injected at t=5.0 sec. At t=5.54 sec, radiated power, P_{rad}, starts to increase and the electron temperature, T_e, at r=80cm starts to decrease. Then P_{rad} continues to increase and T_e in the edge region (r=60 and 80cm) decreases much faster than T_e at the central region. At t=5.6 sec, the Hα signal increases drastically and MARFE occurs. Then, at t=5.615 sec, fluctuation of the poloidal magnetic field with m=2 and m=3 components start to increase. In this time evolution, the trigger (t=5.54sec) of the instability is increase in Prad and decrease in Te(edge). At this time, Prad/Pabs=43%.

Figure 9 gives another disrupted case without long MARFE before the disruption. At t=6.14 sec, T_e at r=80cm happens to decrease and P_{rad} starts to increase. In the low temperature region dominated by line-radiation, decrease in T_e increases P_{rad}. When P_{rad} increases, T_e decreases further. In Fig.9, the trigger of the disruption occurs at t=6.14 sec ,Prad/Pabs =30%, and the power balance in the edge region cannot be stabilized after this time. In the early phase of the edge cooling (6.15 <t<6.18 sec) , the central temperature is not affected. Figure 9(b) shows profiles of radiated power density calculated with a magnetic surface fitting of the measured data for t=6.14 and 6.17 sec. After the degradation of the thermal balance, radiated power increases from the outer portion of the plasma.

Figure 10 plots the relationship between P_{rad} and P_{abs} at the trigger time of the disruption (closed circles) and that for stable discharges (open circles). The broken line in the figure represents Prad=Pabs. For the stable discharges, Prad/Pabs is from 10 to 40%. For the disrupted discharges, the ratio is from 20 to 100%.

3.5 Disruption Limit

The major fraction of the total radiated power is due to that in the edge region. Figure 11 (a) shows the relationship between P_{rad}(total) and n_e^2(r=50cm)×Z_{eff}(r=50cm). The linear dependence indicates that n_e^2(r=50cm)×Z_{eff}(r=50cm) is a good measure of the total radiation power. In Fig.11(b), disrupted and stable discharges are plotted in the space of n_e^2(r=50cm)×Z_{eff}(r=50cm)/P_{abs} and P_{abs}. In this figure, it can be understood that the disruption condition is represented as the result of the degradation of the power balance in the outer region of the plasma and decrease in Z_{eff} and increase in P_{abs} rises the density limit.

3.6 Edge Temperature

To evaluate the radiated power precisely, electron temperature is a key factor in addition to n_e and Z_{eff}, because the radiation power is a strong function of Te. The dominant light impurity

species in JT-60 are carbon and oxygen. For these impurities, the radiation power parameter increases drastically with decrease in T_e at T_e<1 keV. Figures 12(a) and (b) show the range of T_e(r=60cm) at just before the trigger time of the disruption defined in Sec. 3.4 for disrupted and stable discharges. The disrupted data have Te(r=60cm) ranged from 0.4 to 1.3 keV which is systematically lower than that for stable discharges for the same P_{abs} and n_e^2(r=50cm)×Z_{eff} (r=50cm).

3.7 Hugill diagram for OH discharges

Figure 13 is the Hugill diagram for OH limiter discharges. The upper density limit for stable discharges can be written by $n_e(r=50cm)Rq/B_t=12\times10^{19}m^{-2}T^{-1}$. For OH discharges, the parameter nRq/Bt seems a good indication of the density limit for the current carrying toroidal configurations. This is because the similar discussion about values of nRq/Bt or ratio of electron density / current density (ne/j) can describe the density limit for ultra low-q (ULQ; q(a)<1) and reversed field pinch (RFP; q(a)<0) configurations. Figure 14 shows the Hugill diagram for the ultra low-q discharges on REPUTE-1 device [6] . In the The region enclosed by solid lines corresponds to discharges overcoming the radiation barrier. The other group in a higher density range (enclosed by broken lines) corresponds to low temperature (Te ~30~80eV). In the field of RFP research, the upper density limit is known as 'lower-I/N' limit, I and N are the plasma current and line density defined by $n_e\pi a^2$ [7].

4. MARFE Limit

Figure 15 gives the typical time evolution of MARFE. The occurrence of MARFE suppresses the further increase in n_e although the gas-puffing of 12Pam3/sec is added. Figure 16 shows the MARFE limit in JT-60 limiter discharges with gas-puffing. For P_{abs} <15MW and P_{abs}>15MW, the MARFE limits are described by neRq/Bt=14 and $17\times10^{19}m^{-3}T^{-1}$.

5. Fuelling Efficiency

Figure 17 shows the fuelling efficiency of the gas and pellet fuelling. For the gas puffing, the fuelling efficiencies are about 20% and 30% for divertor and limiter configurations. Especially for divertor configuration, the attainable electron density saturate below a low level because of low recycling property [6]. For the pellet injection, the fuelling efficiency is 100% and it is a favorable fuelling scenario for the divertor discharges in JT-60.

6. Conclusion

This report studies mainly the density limit for a series of gas- and pellet-fuelled limiter discharges in JT-60. With the pellet injection into high-current / low-q (q(a)=2.3~2.5) discharges, the Murakami factor reaches up to $10\sim13\times10^{19}m^{-2}T^{-1}$. The values are about factors of 1.5~2.0 higher than those for usual gas-fuelled discharges. The pellet injected discharges have high central density, whereas the electron density in the outer region (a/2<r) is limited below the same level with that for gas fuelled plasmas.The density limit can be explained with the power balance in the outer region of the plasma, for which the plasma purity (Zeff), heating power and the electron temperature are the key parameters. The disruptive limit of the density can be explained by P_{abs} and $n_e^2(r=50cm)\times Z_{eff}(r=50cm)$.

REFERENCES

[1] KAMADA,Y., YOSHINO,R.,NAGAMI,M.,OZEKI,T., HIRAYAMA,T., et al. Nucl. Fusion **29** (1989) 1785

[2] JT-60 Team presented by NAGAMI,M., Plasma Phys. Control. Fusion **31,** (1989) 1597

[3] OZEKI, T., AZUMI.M., KAMADA.Y., et al., submitted to Nucl. Fusion

[4] JT-60 Team, in *Plasma Physics and Controlled Nuclear Fusion Research* (Proc.12th Int. Conf., Nice, 1988) IAEA-CN-50/ A-1-4.

[5] HOSOGANE, N., KAMADA.Y., TUNEMATSU,T., "Density Limit in JT-60" the ITER expert meeting on density limits, Garching, September 20-22, 1989.

[6] KAMADA. Y., FUJITA.T., YOSHIDA, Z., INOUE, N., et al., Nucl. Fusion **29** (1989) 713

[7] ORTOLANI, S., ROSTAGNI, G., Nucl. Instrum. Methods **207** (1983) 35.

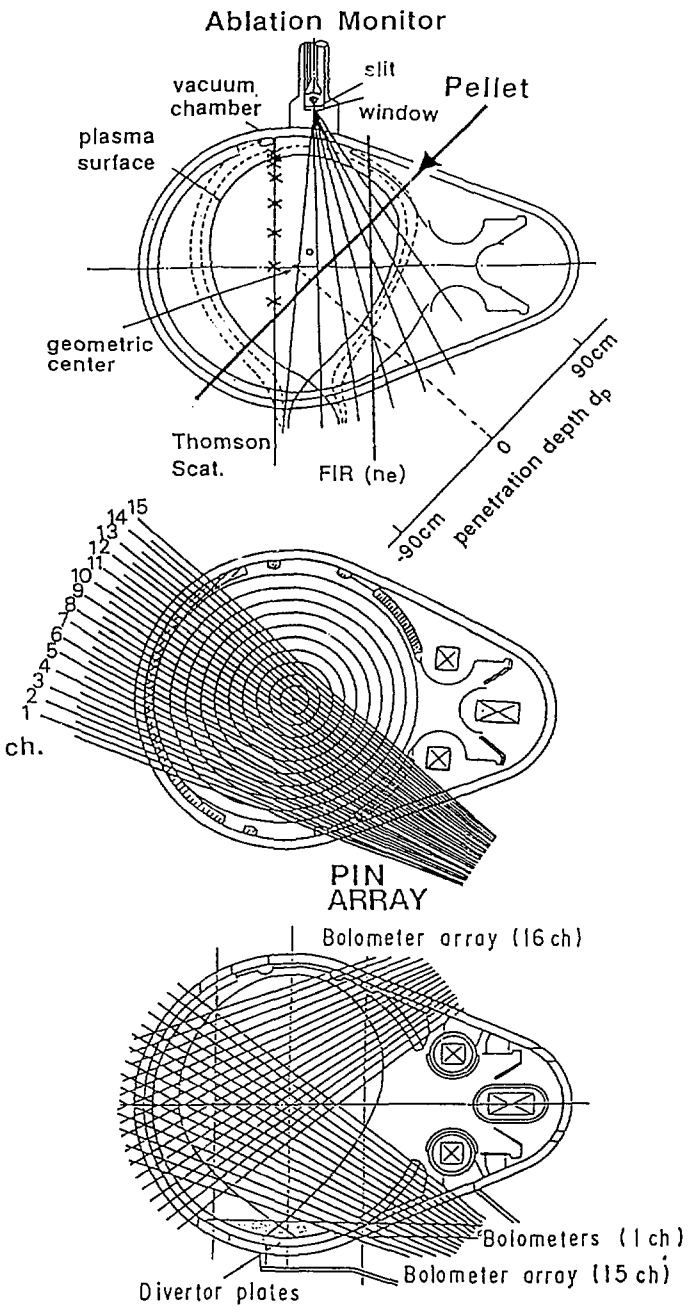

Fig.1 (a) Lower x-point configuration of a JT-60 plasma. Pellet path, lines of sight of the pellet ablation monitor, chords of a Thomson scattering system (measured points are indicated by ×) and a FIR interferometer are shown.
(b) The limiter configuration and lines of sight of a lower half set of soft-X ray detectors.
(c) The bolometer array.

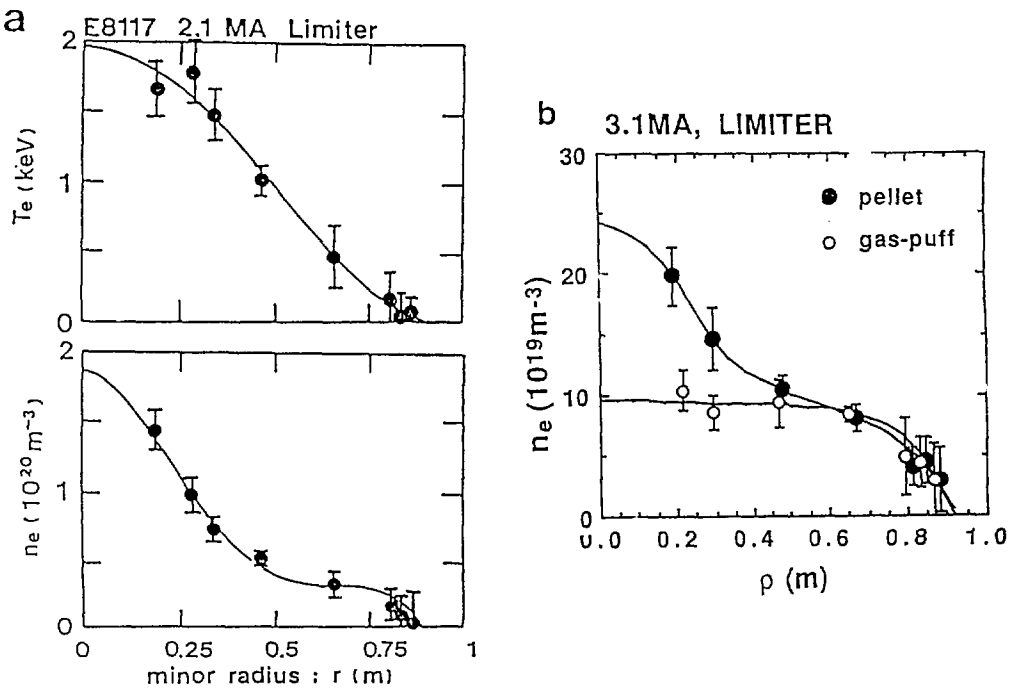

Fig.2 Electron density profiles for pellet fuelled limiter discharges. With the pellet injection, the strongly peaked electron density profile with the peaking factor (central value / volume averaged value) $n_e(0)/\langle n_e \rangle$ <4.5 was obtained for medium current of Ip=2.1MA (q(a)=3.3) (Fig.2(a)). (b) gives an example for $n_e(r)$ for a 3.1MA (q(a)=2.3) limiter discharge, where $n_e(0)/\langle n_e \rangle$ <3 and $n_e(0)<2.7\times10^{20}m^{-3}$ was sustained within 0.5-1 sec after a series of pellet injection. In (b), $n_e(r)$ for a gas fuelled discharge is shown.

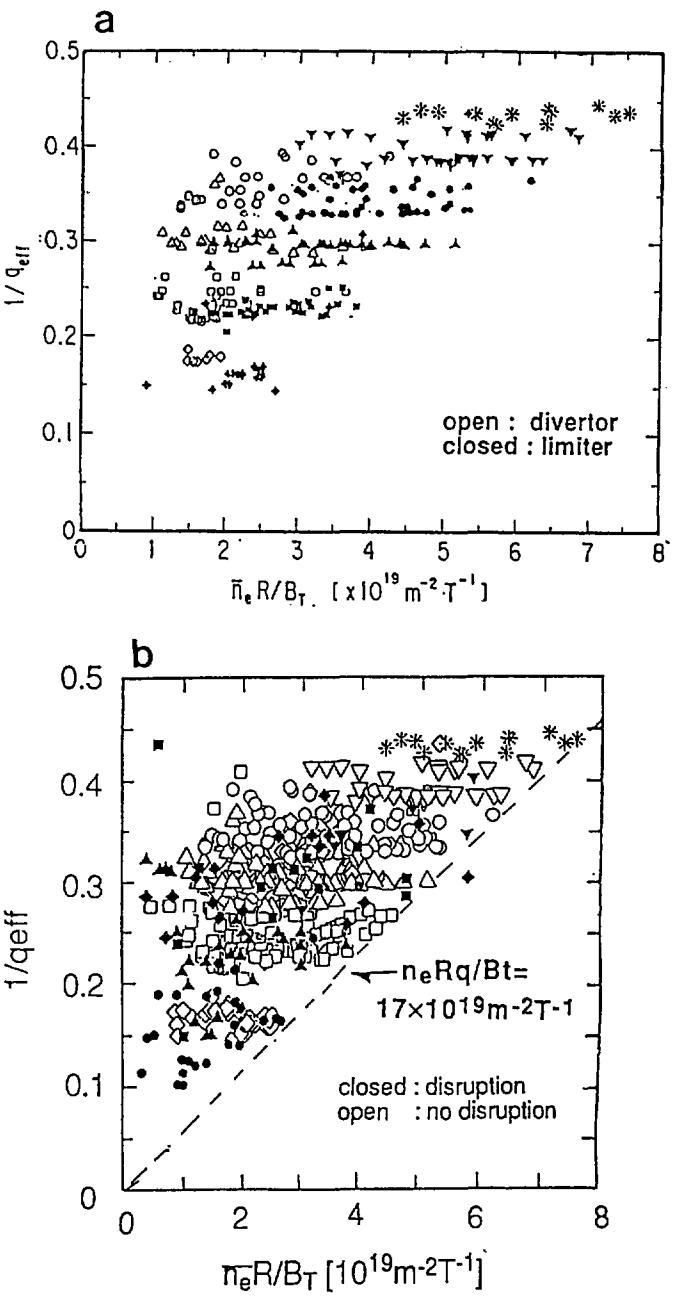

Fig.3 Operational region for gas fuelled plasmas on the Hugill diagram. (a) indicates the operational region for limiter and divertor discharges without disrupted data. In (b), the disrupted data (closed symbols) are plotted on the stable data.

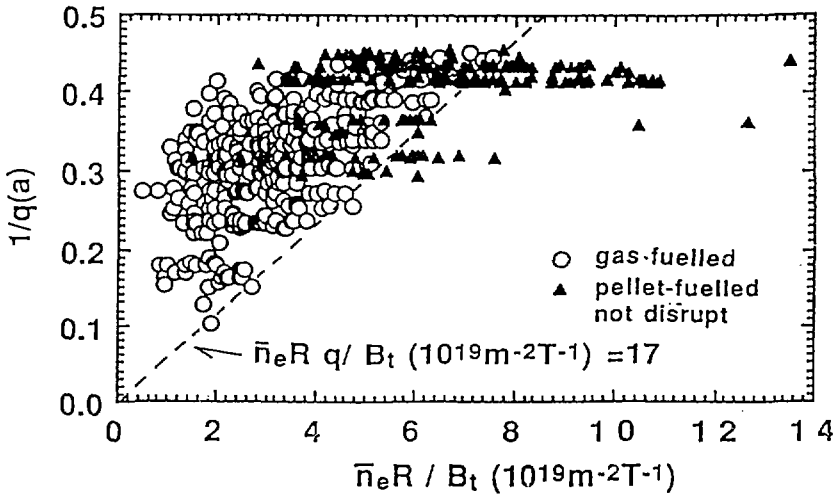

Fig.4 The operational region for pellet fuelled limiter discharges are superimposed on that for the gas fuelled discharges. With the pellet injection into high-current / low-q (q(a)=2.3~2.5) discharges, the Murakami factor reaches up to $10\sim13\times10^{19}m^{-2}T^{-1}$.

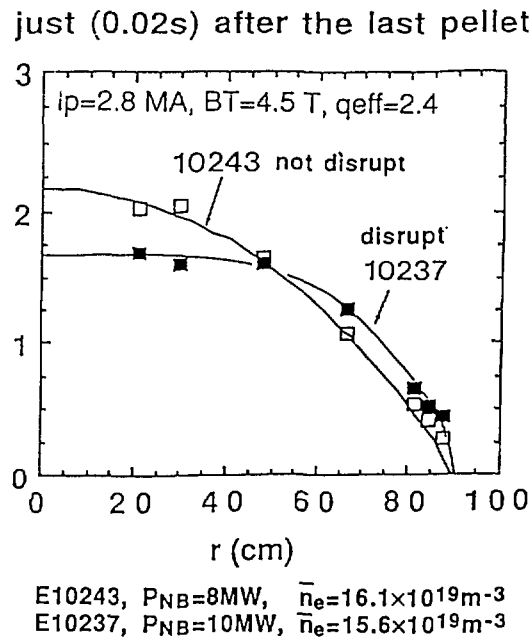

Fig.6 Electron density profiles for 2.8MA limiter discharges measured just (0.02sec) after the pellet injection. E10243 was stable and E10237 disrupted at 0.1 sec after the pellet injection.

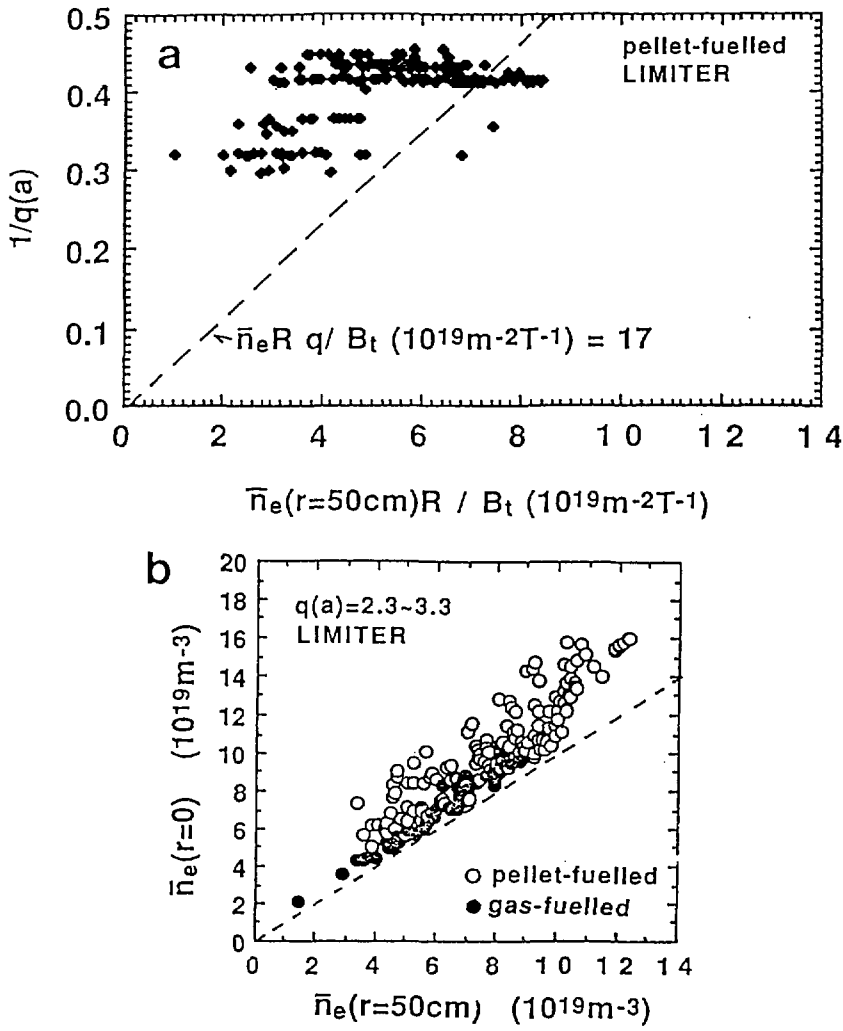

Fig.5 (a) Hugill diagram of pellet discharges with line averaged electron density for the 50cm-off-axis chord, n_e(r=50cm).
(b) Comparison with the line averaged n_e for the central and the off-axis chords in the range of 2.3<q(a)<3.3.

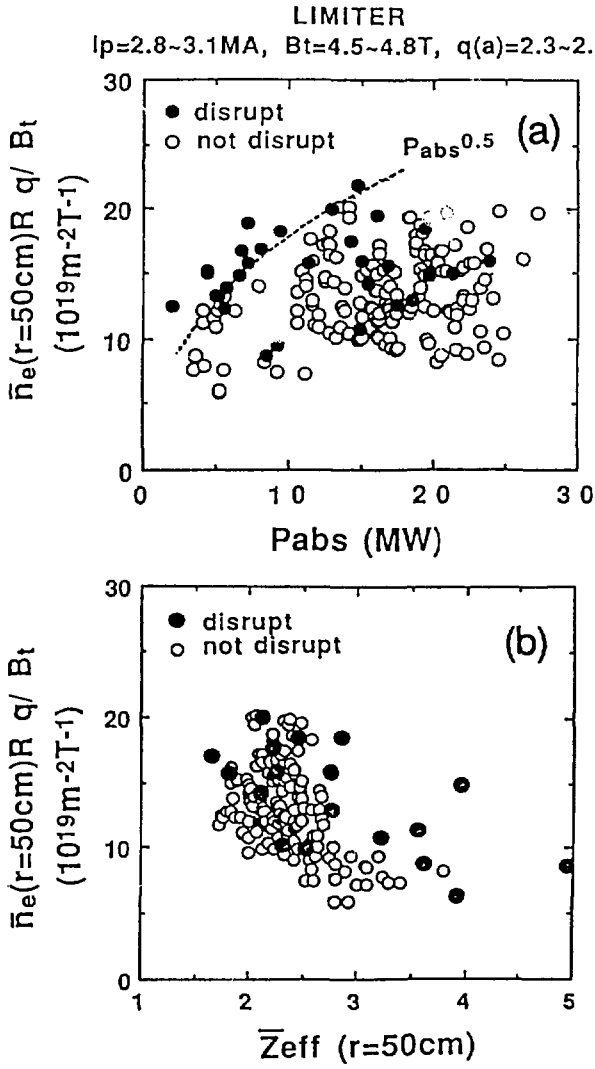

Fig.7 n_e(r=50cm)Rq/Bt against absorbed power P_{abs} and Z_{eff} averaged along the 50cm-off-axis chord for gas and pellet fuelled limiter discharges with Ip=2.8~3.1MA, Bt=4.5~4.8T and q(a)=2.3~2.4.

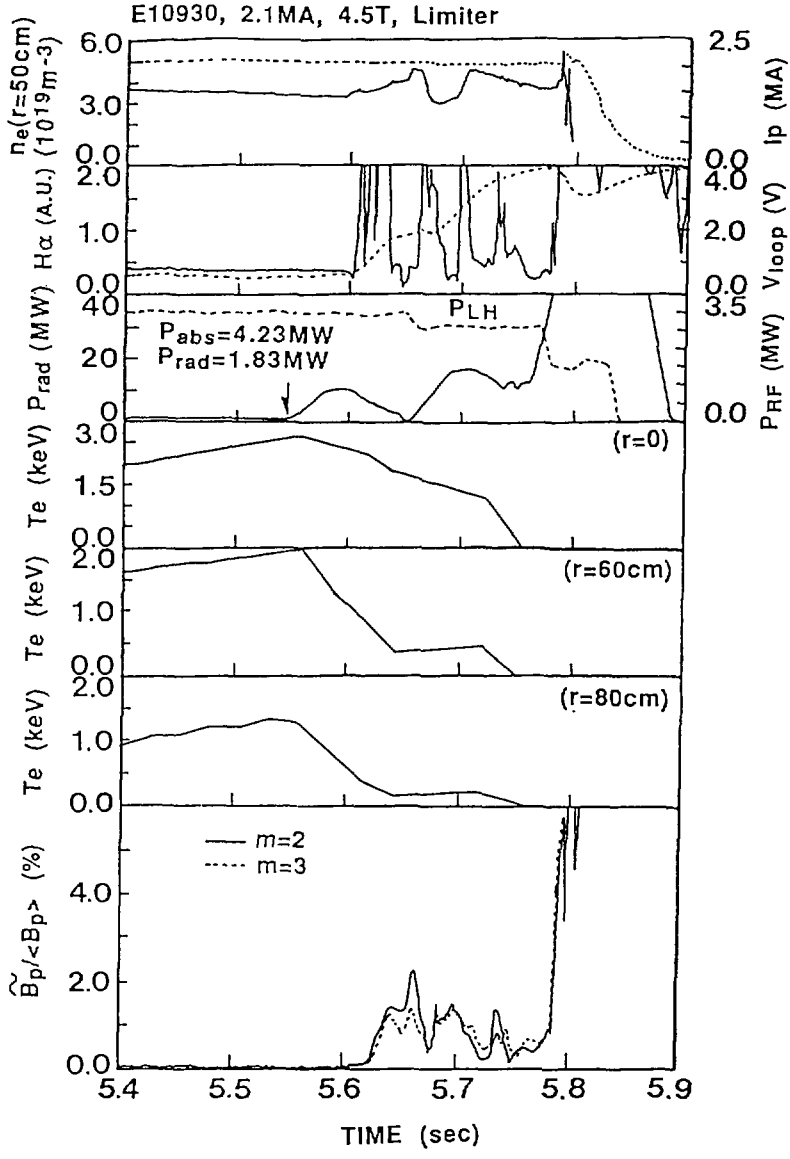

Fig.8 The time evolution of the density limit disruption for a 2.1MA limiter discharge, in this case the pellets were injected at t=5.0 sec.

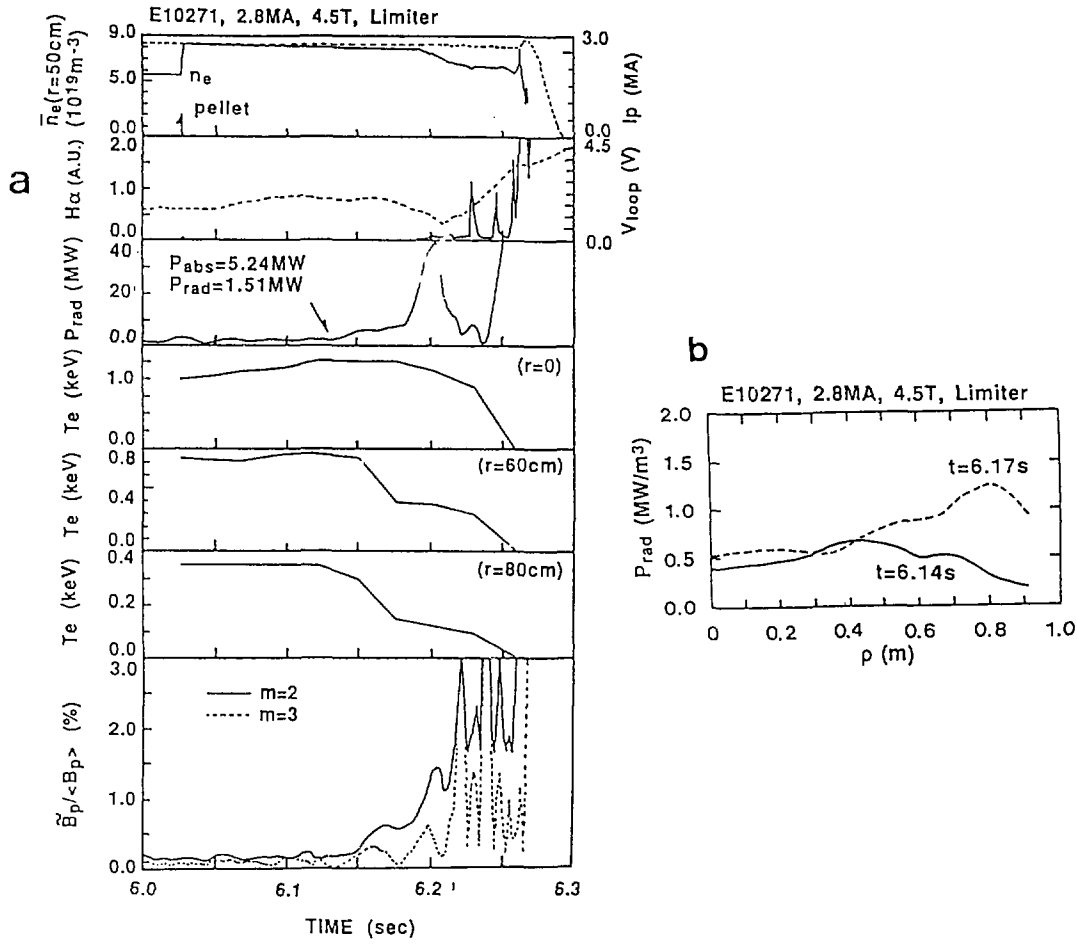

Fig 9 (a) The time evolution of the density limit disruption for a 2.8MA limiter discharge. without long MARFE before the disruption.
(b) The profiles of radiated power density calculated with a magnetic surface fitting of the measured data for t=6.14 and 6.17 sec.

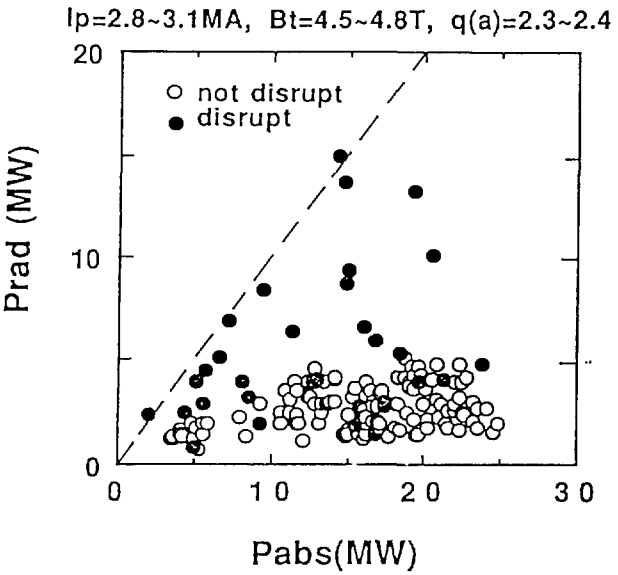

Fig.10 The relationship between P_{rad} and P_{abs} at the trigger time of the disruption (closed circles) and that for stable discharges (open circles) for gas and pellet fuelled limiter discharges with Ip=2.8~3.1MA, Bt=4.5~4.8T and q(a)=2.3~2.4.

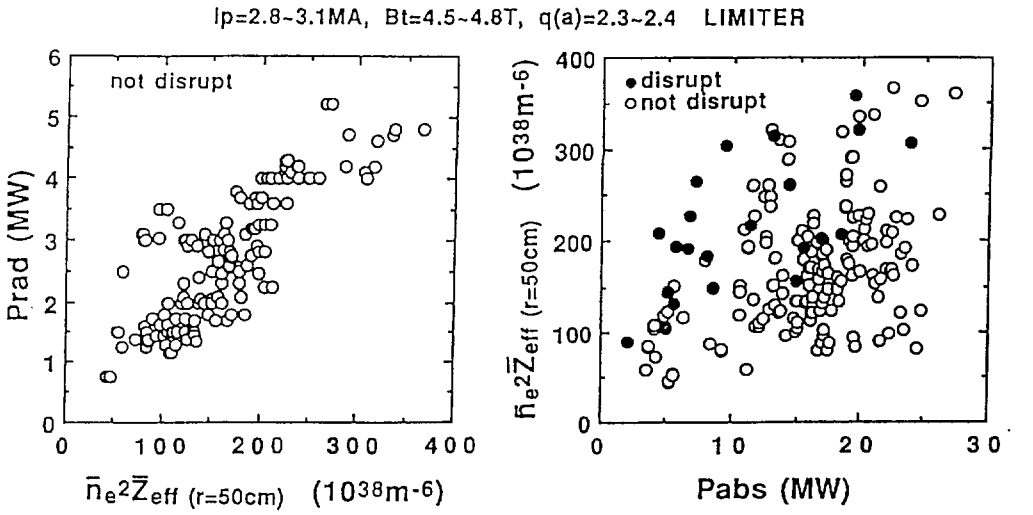

Fig.11 (a) Relationship between P_{rad}(total) and n_e^2(r=50cm)×Z_{eff}(r=50cm). The linear dependence indicates that n_e^2(r=50cm)×Z_{eff}(r=50cm) is a good measure of the total radiation power.
(b) Disrupted (closed circle) and stable (open circle) discharges in the space of n_e^2(r=50cm)×Z_{eff}(r=50cm) and P_{abs}. (Data plotted are from gas and pellet fuelled limiter discharges with Ip=2.8~3.1MA, Bt=4.5~4.8T and q(a)=2.3~2.4).

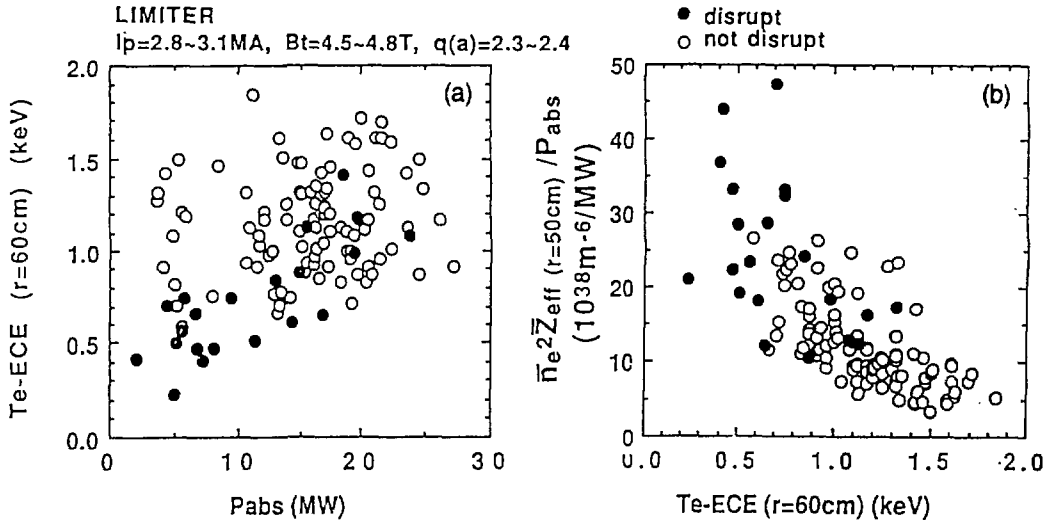

Fig12 Relationships of (a)T_e(r=60cm) vs P_{abs} and
(b) n_e^2(r=50cm)×Z_{eff}(r=50cm)/P_{abs} vs T_e(r=60cm)
at just before the trigger time of the disruption for gas and pellet fuelled limiter discharges with Ip=2.8~3.1MA, Bt=4.5~4.8T and q(a)=2.3~2.4.

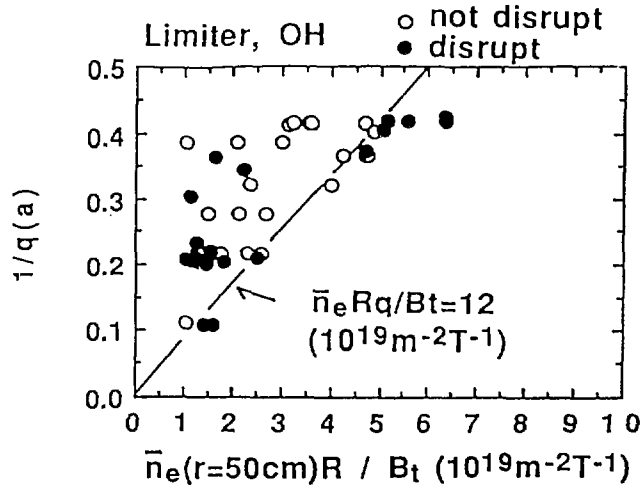

Fig13 Hugill diagram for OH limiter discharges.
The upper density limit for stable discharges can be written by n_e(r=50cm)Rq/B_t=12×10^{19}m^{-2}T^{-1}.

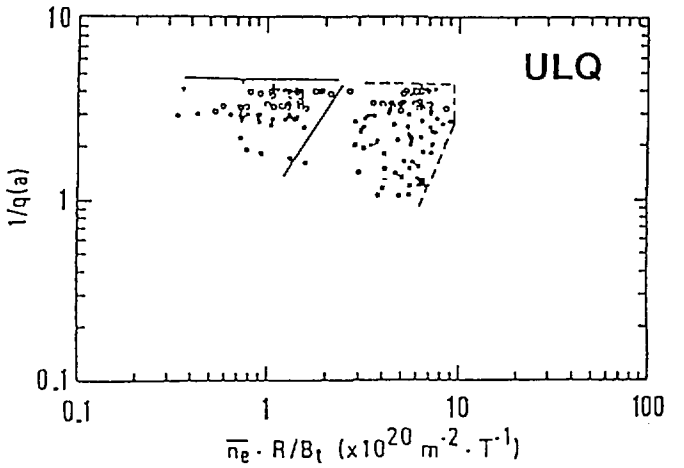

Fig.14 Hugill diagram for the ultra low-q discharges on REPUTE-1 device [7]. In the region enclosed by solid lines corresponds to discharges overcoming the radiation barrier. The other group in a higher density range (enclosed by broken lines) corresponds to low temperature (Te ~30~80eV).

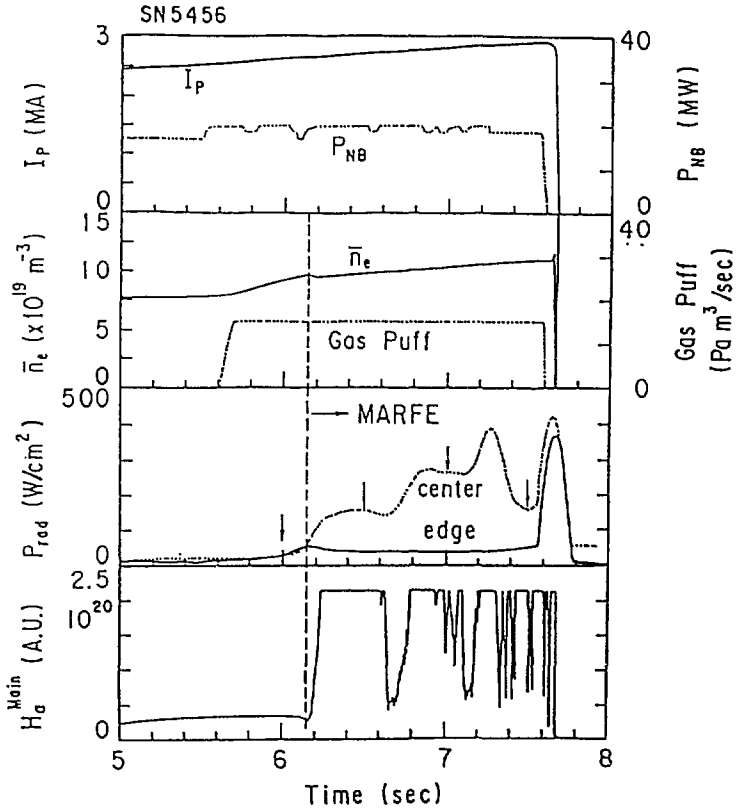

Fig.15 The typical time evolution of MARFE. The occurrence of MARFE suppresses the further increase in n_e although the gas-puffing of 12Pam3/sec is added.

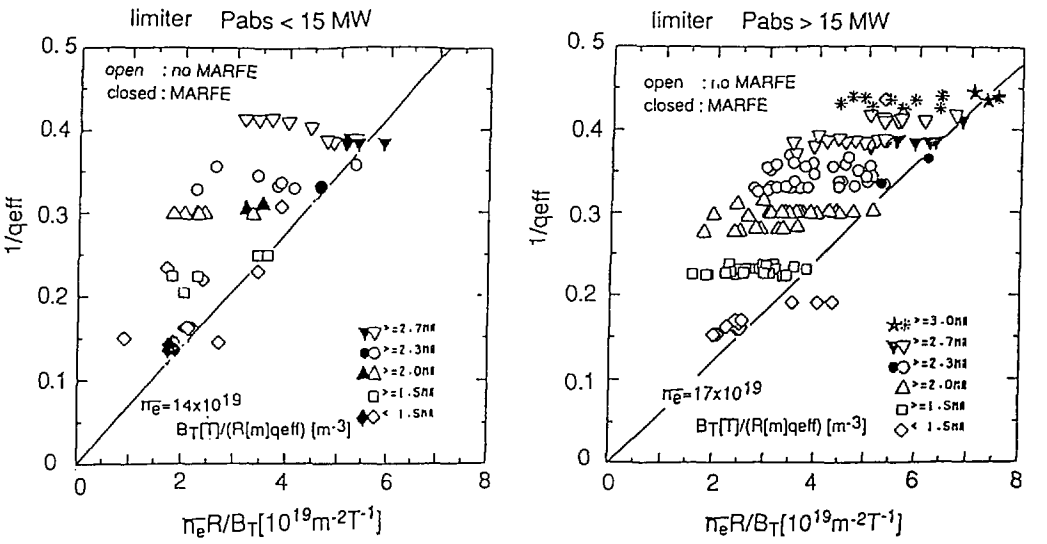

Fig.16 The MARFE limit in JT-60 limiter discharges with gas-puffing. For P_{abs} <15MW and P_{abs}>15MW, the MARFE limits are described by neRq/Bt=14 and 17×10^{19}m^{-3}T^{-1}.

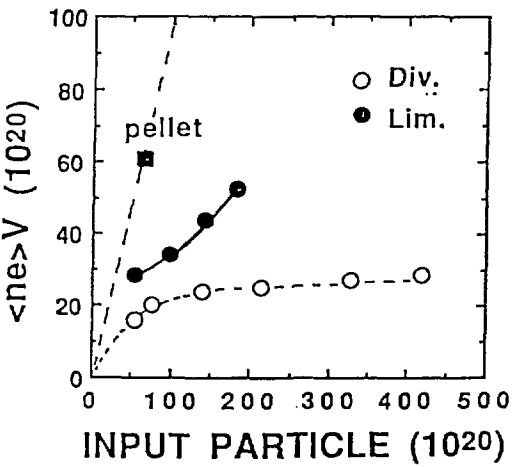

Fig.17 The fuelling efficiency of the gas and pellet fuelling.